photonics

MDPI

Article

PPB-Level Detection of Dissolved Acetylene in Transformer Oil Based on a Clamp-Type Quartz-Enhanced Photoacoustic Spectroscopy System

Yihua Qian [1], Yaohong Zhao [1,*], Qing Wang [1], Kun Jia [2], Guobin Zhong [2] and Huadan Zheng [2]

[1] Guangdong Key Laboratory of and Electric Power Equipment Reliability, Electric Power Research Institute of Guangdong Power Grid Co., Ltd., Guangzhou 510060, China; 13926035192@163.com (Y.Q.); sdytwangqing@163.com (Q.W.)
[2] National Institute of Guangdong Advanced Energy Storage, Guangzhou 510000, China; jiakun1118@163.com (K.J.); zhongguobin001@163.com (G.Z.); zhenghuadan@jnu.edu.cn (H.Z.)
* Correspondence: kennyaoo@126.com

Abstract

Dissolved gas analysis (DGA) is an essential technique for the fault diagnosis and condition monitoring of oil-immersed power transformers. Among various characteristic gases, acetylene (C_2H_2) is a key indicator of high-energy discharge and arc faults. In this work, a high-sensitivity dissolved acetylene detection system is developed based on clamp-type quartz-enhanced photoacoustic spectroscopy (QEPAS). A specially designed clamp-type quartz tuning fork (Clamp-type QTF) is employed as the acoustic transducer to improve acoustic coupling efficiency and optical alignment tolerance. Compared with conventional standard quartz tuning forks, the clamp-type structure exhibits enlarged acoustic interaction volume, lower damping loss, and higher signal collection capability. A near-infrared distributed feedback (DFB) laser operating at 1531.6 nm is used as the excitation source. The dissolved gas is extracted from transformer oil using a headspace degassing module and introduced into the QEPAS cell for real-time measurement. Experimental results showed that the developed system achieves a 1σ-based SNR-estimated detection limit of 17 ppb at a 50 s integration time, derived from the continuous measurement of 0.75 ppm C_2H_2, with excellent linearity in the concentration range from 100 ppm to 500 ppm. The measured concentration of dissolved acetylene in transformer oil is in good agreement with gas chromatography (GC), validating the effectiveness and practical applicability of the proposed system.

Keywords: quartz-enhanced photoacoustic spectroscopy; photoacoustic spectroscopy; quartz tuning fork; gas sensor

Check for updates

Received: 13 April 2026
Revised: 22 May 2026
Accepted: 26 May 2026
Published: 1 June 2026

Copyright: © 2026 by the authors. Licensee MDPI, Basel, Switzerland. This article is an open access article distributed under the terms and conditions of the Creative Commons Attribution (CC BY) license.

1. Introduction

Dissolved gas analysis (DGA) has been widely recognized as an essential technique for condition monitoring and fault diagnosis of oil-immersed power equipment [1–3]. During long-term operation, abnormal conditions such as partial discharge, local overheating, and arc faults cause the thermal decomposition of insulating oil and solid insulating materials, resulting in the generation of various characteristic dissolved gases [4,5]. Among them, acetylene (C_2H_2) is considered a critical indicator gas for high-energy discharge faults. Therefore, achieving highly sensitive and selective detection of acetylene at the ppb level is

of great significance for early fault warning and operational reliability assessment of power transformers [6,7].

At present, several techniques have been employed for dissolved gas detection, including gas chromatography, chemical sensors, Tunable Diode Laser Absorption Spectroscopy, infrared sensing, and photoacoustic spectroscopy (PAS) [8,9]. Among these methods, PAS has attracted increasing attention in recent years due to its outstanding advantages in trace gas detection, including high sensitivity, excellent selectivity, and strong compatibility with laser sources [10,11]. In particular, the use of laser excitation significantly enhances both the sensitivity and molecular selectivity of the system [12,13]. More importantly, one of the key characteristics of PAS is its capability to operate with extremely small sampling volumes, which is particularly advantageous for micro-volume gas detection. It should be noted that the photoacoustic signal is not solely determined by the sampling volume, but is fundamentally governed by the optical absorption coefficient, the efficiency of vibrational-to-translational (V–T) relaxation processes, and the acoustic resonance conditions of the system. These features collectively enable PAS to be especially suitable for dissolved gas analysis in transformer oil [4,5].

Photoacoustic spectroscopy is a gas sensing technique based on the photoacoustic effect, first discovered by Alexander Graham Bell in the 19th century [14,15]. Its fundamental principle can be described as follows: when a modulated laser beam at a specific wavelength interacts with target gas molecules, the molecules absorb the optical energy and are excited from the ground state to an upper energy state [16]. Subsequently, these excited molecules relax back to the ground state through collisional de-excitation, converting the absorbed optical energy into thermal energy [17,18]. This process induces periodic temperature fluctuations in the surrounding medium, synchronized with the laser modulation frequency, which further leads to periodic thermal expansion and contraction, thereby generating acoustic waves [19–21]. By detecting these acoustic signals with an appropriate acoustic transducer, the gas concentration can be quantitatively determined [22]. The QEPAS signal amplitude can be approximately expressed as

$$S_{QEPAS} = K \cdot P \cdot \alpha(v) \cdot \frac{Q}{f_0} \cdot F(\tau, f_0, p) \quad (1)$$

where K is a system-dependent constant related to acoustic coupling and piezoelectric transduction, P is the effective laser power, $\alpha(\nu)$ is the absorption coefficient of the target gas at optical frequency ν, Q and f_0 are the quality factor and resonance frequency of the QTF, respectively, and $F(\tau, f_0, p)$ describes the influence of molecular relaxation time τ and pressure p. The absorption coefficient is given by

$$\alpha = N \cdot \sigma(v) \quad (2)$$

where N is the molecular number density and $\sigma(\nu)$ is the absorption cross-section of acetylene.

Over the past decades, PAS has evolved into several different forms, including microphone-based PAS, resonant PAS, fiber-optic PAS, and quartz-enhanced photoacoustic spectroscopy (QEPAS) [23,24]. Among them, QEPAS, first proposed in 2002 by the group of Frank K. Tittel at Rice University, has become one of the most prominent techniques for ultra-trace gas detection [25,26]. In QEPAS, a quartz tuning fork (QTF) is employed as the acoustic transducer instead of a conventional microphone. Owing to the piezoelectric effect of quartz, the acoustic wave is directly converted into an electrical signal [27]. Compared with traditional PAS systems, QEPAS offers several significant advantages, including an extremely high-quality factor (Q-factor), ultra-small effective sampling volume, and ex-

cellent immunity to environmental acoustic noise [28]. Since the QTF only resonates at a specific frequency, acoustic disturbances outside the resonance frequency are effectively suppressed, leading to substantially improved sensitivity and signal-to-noise ratio [29,30]. These features make QEPAS highly advantageous for DGA, seawater dissolved gas sensing, and other trace gas analysis applications [31–33].

However, conventional QTF-based QEPAS systems still suffer from an intrinsic limitation. The gap between the prongs of a standard commercial 32.768 kHz QTF is typically only 200–300 μm, which imposes stringent requirements on the laser beam quality and optical alignment [34]. Any scattered light or direct illumination on the QTF surface may induce photothermal background noise, thereby severely degrading the detection sensitivity. To address this issue, several research groups have proposed customized QTF structures with enlarged prong spacing [35]. For example, in 2014, Vincenzo Spagnolo and co-workers developed specially designed QTFs with larger spacing to improve the compatibility with different laser beam profiles. In China, researchers from Harbin Institute of Technology have also proposed specially engineered QTF structures to further enhance sensor performance [36,37].

Recently, our group proposed a novel clamp-type quartz tuning fork (Clamp-type QTF) structure to overcome the above limitations [12]. Compared with previously reported customized QTFs, the proposed structure exhibits several unique advantages. First, it provides a significantly larger prong spacing, which effectively reduces optical background noise and relaxes the requirements for laser beam alignment [38]. Second, the inner sidewall geometry of the clamp-type structure is designed to better match the cylindrical acoustic wavefront, thus improving the acoustic coupling efficiency [39]. More importantly, this structure can be fabricated based on a commercially available standard 32.768 kHz quartz crystal resonator, which greatly reduces fabrication cost while maintaining a high Q-factor [40,41].

In this work, a clamp-type QTF was employed as the acoustic transducer to develop a QEPAS-based sensing system for dissolved acetylene detection in transformer oil. A near-infrared distributed feedback semiconductor laser operating at approximately 1.53 μm was used as the excitation source. In addition, a headspace degassing device was designed to efficiently extract acetylene from transformer oil and directly deliver it into the developed clamp-type QTF-enhanced photoacoustic detection system. Experimental results demonstrated a detection sensitivity at the level of several tens of ppb, indicating the great potential of the proposed system for high-sensitivity, low-cost online monitoring of transformer faults.

2. Experimental Setup

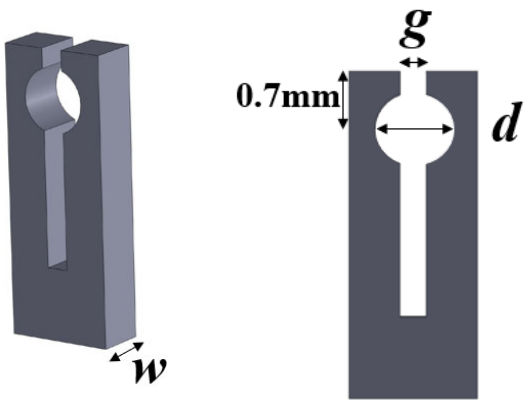
The electrical resonance characteristics of a standard commercial quartz crystal resonator were first characterized to obtain its intrinsic parameters [42]. A packaged standard 32.768 kHz quartz crystal resonator was employed as the initial device. An electrical excitation method was adopted for frequency response measurement [43]. Specifically, a sinusoidal signal with constant amplitude and continuously tunable frequency was generated by a function generator and applied to the electrodes of the quartz resonator. The output response amplitude at different excitation frequencies was recorded using a lock-in amplifier, thereby obtaining the resonance curve [44].

A Lorentzian fitting was then applied to the measured resonance curve to determine the central resonance frequency f_0. The quality factor (Q-factor) was calculated based on the full width at half maximum (FWHM) using

$$Q = \frac{f_0}{\Delta f} \tag{3}$$

where Δf represents the frequency bandwidth at half maximum [45].

After characterizing the original resonator, the standard quartz crystal was structurally modified following the method previously developed by our group. A combination of ultraviolet femtosecond laser micromachining and active chemical etching feedback was employed to reconstruct the prong structure, resulting in a novel clamp-type quartz tuning fork (Clamp-type QTF). The fabricated structure is shown in Figure 1. Key geometric parameters, including the prong spacing, aperture size, and prong tip dimensions, were measured under an optical microscope [46].

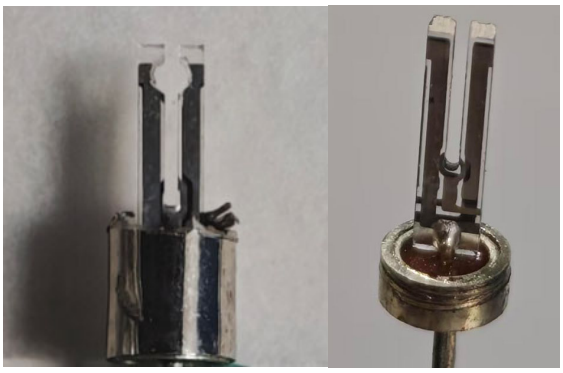


(**a**) (**b**)

Figure 1. (**a**) Clamp-type QTF setup diagram; (**b**) front view of clamp-type QTF. d: the aperture diameter. g: prong spacing. w: prong width. and aperture position: 0.7 mm to the top of the clamp-type QTF.

The fabricated clamp-type QTF was subsequently characterized using the same electrical excitation and Lorentzian fitting method to determine its resonance frequency and Q-factor, thereby evaluating the effect of structural modification on its resonance performance [47].

Following the QTF characterization, a clamp-type QTF-enhanced photoacoustic spectroscopy system was established, as illustrated in Figure 2. The system mainly consists of a gas delivery module, laser excitation module, photoacoustic detection module, and vacuum control module.



(**a**) (**b**)

Figure 2. (**a**) Schematic diagram of the clamp-type QTF-enhanced QEPAS experimental setup; (**b**) schematic diagram of the standard QTF-enhanced QEPAS experimental setup.

The excitation source was a near-infrared distributed feedback diode laser operating at approximately 1531.6 nm, corresponding to an absorption band of acetylene. The laser injection current was sinusoidally modulated for wavelength modulation spectroscopy. Since

the QEPAS signal was detected in the second-harmonic mode, the modulation frequency was set to half of the QTF resonance frequency. The QTF resonance frequency was measured to be 34,911 Hz under atmospheric pressure and shifted to approximately 34,918 Hz at −675 Torr. Unless otherwise specified, all negative pressure values reported in this work are gauge pressures relative to atmospheric pressure. During pressure optimization, the strongest 2f signal was obtained at −637.5 Torr, and this pressure was therefore selected as the optimal working pressure for subsequent measurements. The lock-in amplifier was used to demodulate the second-harmonic signal, and its integration time was set to 1 s during the signal acquisition.

For gas-phase calibration, certified 1000 ppm C_2H_2 standard gas was diluted with 99.99% high-purity N_2 using two mass flow controllers supplied by Sevenstar Huachuang. The desired acetylene concentrations were generated by adjusting the two-channel gas flow ratio between C_2H_2 and N_2. The target concentration was calculated according to the flow-rate ratio of the 1000 ppm C_2H_2 standard gas and the dilution N_2. During calibration, the total gas flow rate was kept constant to minimize flow-induced acoustic disturbance in the QEPAS detection cell. The accuracy of the mass flow controllers was specified by the manufacturer and is reported in the revised Experimental Setup section. A near-infrared distributed feedback (DFB) semiconductor laser operating at approximately 1531.6 nm was used as the excitation source, corresponding to the characteristic absorption line of acetylene molecules [48].

The laser beam, modulated by a sinusoidal current signal, was collimated and directed into the acoustic detection region. After passing through the micro-resonator, the beam was focused into the prong gap of the clamp-type QTF, where the target gas generated periodic photoacoustic signals. A pair of stainless-steel cylindrical acoustic micro-resonators was placed symmetrically on both sides of the clamp-type QTF to form an on-beam QEPAS configuration. The laser beam passed coaxially through the resonator and the QTF aperture. The inner diameter and outer diameter of each resonator were 1.0 mm and 1.2 mm, respectively, and the length of each resonator was 4.1 mm. The distance between the resonator end and the QTF plane was maintained at approximately 20 μm. Compared with the bare clamp-type QTF, the acoustic micro-resonator enhanced the 2f photoacoustic signal by a factor of 10 times, indicating improved acoustic confinement and coupling efficiency. This configuration confines the photoacoustic wave around the optical excitation path and enhances the acoustic coupling to the QTF vibration mode. These acoustic signals were converted into electrical signals by the piezoelectric effect of the QTF and subsequently demodulated as second harmonic (2f) signals using a preamplifier and lock-in amplifier.

A vacuum pump and precision needle valve were connected to the outlet of the system to regulate the working pressure inside the detection cell. The pressure was continuously monitored using a high-precision vacuum gauge [49,50].

For practical dissolved gas analysis in transformer oil, a headspace degassing platform was further developed, as shown in Figure 3. The setup mainly consists of a vacuum pump, pressure gauge, oil mist separator, degassing chamber, and clamp-type QTF photoacoustic detection module. The vacuum pump was used to establish a negative-pressure environment, while the pressure gauge continuously monitored the internal pressure. The oil mist separator prevented oil vapor from entering the detection cell and contaminating the QTF. The degassing chamber was composed of a sealed cover and tank body, equipped with gas inlet, gas outlet, and oil inlet ports, enabling direct connection to the transformer oil circulation system.

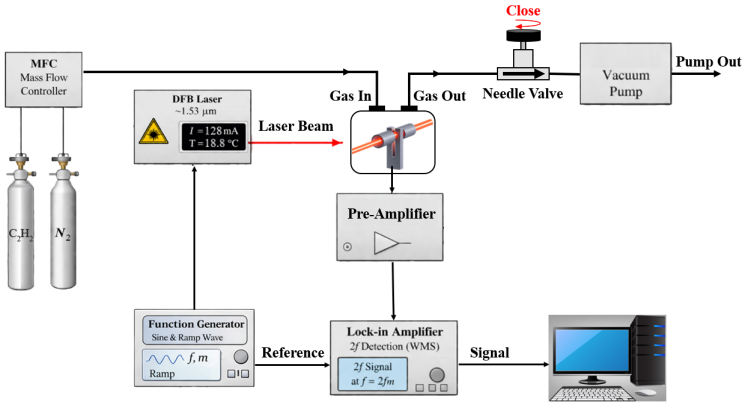


Figure 3. Schematic diagram of quartz-enhanced photoacoustic spectroscopy experimental system based on clamp-type QTF.

For headspace degassing, the distribution of acetylene between transformer oil and the gas phase can be described by gas–liquid equilibrium. At equilibrium, the concentration in the headspace is related to the dissolved concentration in oil through a temperature-dependent partition coefficient. The extraction fraction can be expressed as

$$\eta = \frac{KV_g}{V_0 + KV_g} \tag{4}$$

where K is the oil-gas partition coefficient, V_g is the headspace volume, and V_o is the oil volume. Under negative pressure, the reduced acetylene partial pressure in the headspace promotes desorption from oil. The dynamic degassing process can be approximately described by

$$C_g(t) = C_{g,eq}[1 - \exp(-k_m t)] \tag{5}$$

where k_m is an effective mass-transfer coefficient.

The measurement procedure was as follows: the system was first cleaned with the oil sample, followed by evacuating the degassing chamber to −735 Torr. Then, 500 mL of transformer oil was injected into the chamber using an oil pump. The chamber was evacuated again to the target negative pressure, after which the vacuum pump was kept running to maintain internal gas circulation. Finally, the laser detection system was activated for real-time measurement. All experiments were conducted under laboratory room-temperature conditions. During gas-phase calibration, high-purity N_2 was used as the dilution gas, which minimized humidity-related interference. Although no additional humidity control module was used in the present laboratory setup, humidity effects were largely suppressed because the calibration gas matrix was dry N_2. It should be noted that temperature variations may affect the laser wavelength, QTF resonance frequency, gas absorption linewidth, and oil-gas partition equilibrium in the headspace degassing process. Therefore, temperature monitoring and compensation should be considered in future field-deployment systems to improve long-term measurement stability and accuracy.

3. Results and Discussion

3.1. Quartz Tuning Fork Characterization

The resonance characteristics of the fabricated clamp-type QTF were first investigated. A standard 32,768 kHz quartz crystal resonator was tested using an electrical excitation method. A sinusoidal signal with constant amplitude and tunable frequency was applied to the resonator via a function generator, and the output amplitude was recorded using a lock-

in amplifier. The resonance curve was fitted with a Lorentzian function to determine the central frequency f_0 and FWHM, from which the quality factor (Q-factor) was calculated.

The novel clamp-type QTF was fabricated using ultraviolet femtosecond laser micromachining combined with active chemical etching feedback. The resulting structure is shown in Figure 1, with prong spacing, aperture size, and tip dimensions measured under a microscope. Electrical characterization confirmed that the modified QTF exhibited an increased Q-factor and a resonance frequency shift from 32,768 Hz to 34,911 Hz, indicating improved acoustic energy confinement and improved acoustic coupling efficiency.

3.2. Pressure and Modulation Optimization

Because the photoacoustic signal is highly sensitive to working pressure, the QTF performance was evaluated under different pressures. The internal pressure of the detection cell was adjusted from low pressure to atmospheric pressure, and corresponding resonance curves were measured in Figure 4a. Results showed that under low pressure, gas damping decreased, leading to narrower FWHM, higher Q-factor, and a resonance frequency shift from 34,911 Hz to 34,918 Hz, as shown in Figure 4b.

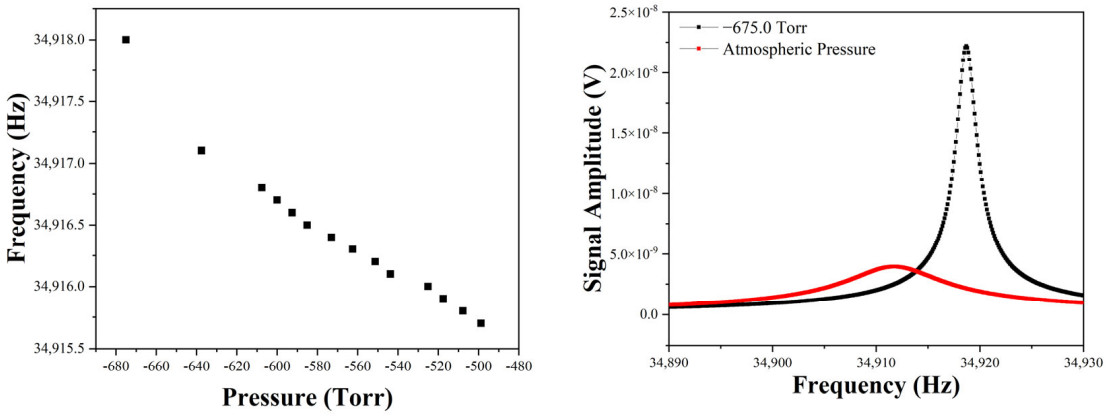


Figure 4. (**a**) Resonant frequency curve under different pressures; (**b**) resonant frequency curve between atmospheric pressure and −675 Torr.

It should be noted that the optimal pressure for QEPAS detection is not determined solely by the QTF resonance amplitude or Q-factor. Although reducing the pressure can decrease gas damping and enhance the QTF resonance response, an excessively low pressure also reduces the molecular number density in the detection cell, thereby weakening the generated photoacoustic wave. In addition, pressure variations can influence the absorption linewidth and molecular relaxation process of acetylene, which further affects the second-harmonic QEPAS signal. Therefore, the final signal amplitude is governed by the combined effects of QTF resonance enhancement, gas molecular density, absorption linewidth, and relaxation dynamics.

The optimal modulation depth for the maximum 2f photoacoustic signal was determined at four different pressures, as shown in Figure 5. To determine the practical optimal operating pressure, the 2f photoacoustic signal was experimentally measured under different pressures and modulation amplitudes, as shown in Figure 5. The results show that the signal amplitude did not increase monotonically with decreasing pressure, but exhibited a maximum at an intermediate negative pressure. Among the tested pressure conditions, the strongest 2f signal was obtained at −637.5 Torr. Therefore, −637.5 Torr was selected as the optimal working pressure for subsequent gas calibration and dissolved acetylene measurements. Each pressure had a corresponding optimal modulation depth, with lower

pressures requiring smaller modulation. Based on signal amplitude and system stability, the optimal operating condition was chosen as −637.5 Torr.

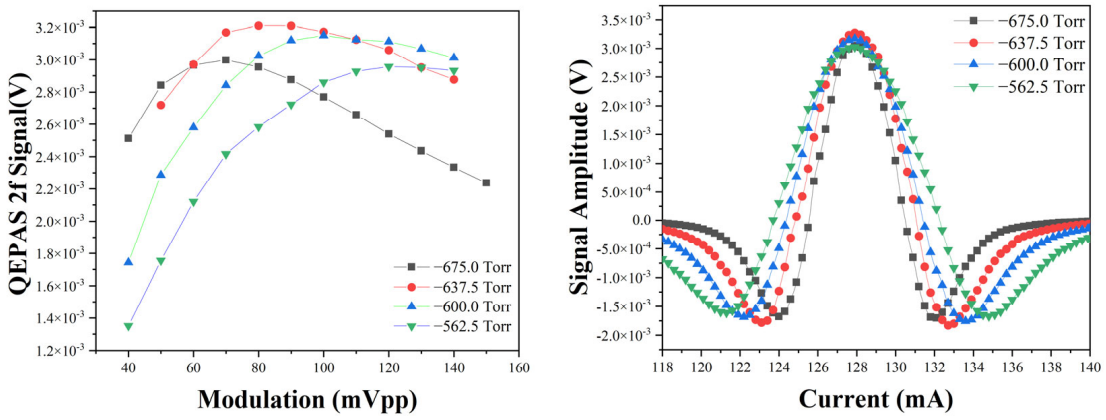


Figure 5. (**a**) Optimal modulation amplitude curves of the photoacoustic signal under different pressures; (**b**) 2f signals of 500 ppm acetylene at the optimal modulation amplitude under different pressures.

3.3. Gas-Phase Calibration

The system's quantitative performance was validated using standard acetylene gas in the range of 100–500 ppm. The measured 2f signals are shown in Figure 6a, with the horizontal axis representing laser output current (or scanning wavelength) and the vertical axis representing the voltage signal. Linear fitting results demonstrated excellent linearity over the 100–500 ppm range, with a correlation coefficient of 0.999 as shown in Figure 6b.

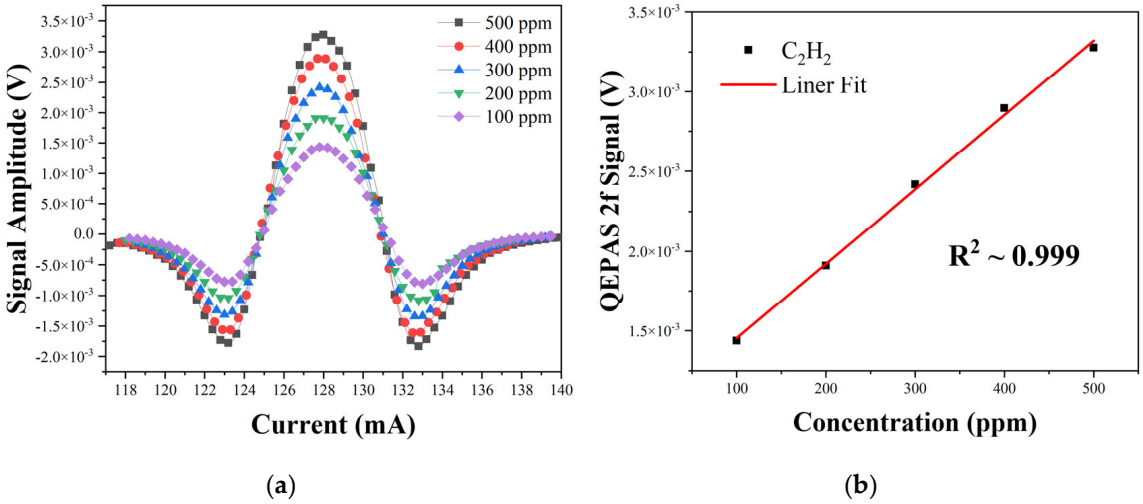


Figure 6. (**a**) Second-harmonic (2f) signals of acetylene at different concentrations under a pressure of −637.5 Torr; (**b**) linear fitting curve of the 2f signal amplitude versus acetylene concentration under −637.5 Torr.

Integration time significantly affects the noise level and signal stability of the QEPAS system. A 50 s integration time was used to reduce signal fluctuation and improve the stability of the measured 2f signal. To evaluate the detection limit, a low-concentration 0.75 ppm C_2H_2 sample diluted in high-purity N_2 was continuously measured under the optimized operating conditions.

The limit of detection (LOD) was estimated based on the signal-to-noise ratio (SNR) of the continuous 0.75 ppm C_2H_2 measurement, rather than by directly measuring a 17 ppb C_2H_2 sample. Specifically, the SNR was calculated by dividing the mean signal amplitude of the 0.75 ppm C_2H_2 response by the standard deviation of the same continuous signal segment:

$$SNR = \frac{\bar{S}_{0.75ppm}}{\sigma_{0.75ppm}} \tag{6}$$

where $\bar{S}_{0.75\,ppm}$ is the mean signal amplitude of the 0.75 ppm C_2H_2 measurement under a 50 s integration time, and $\sigma_{0.75ppm}$ is 1σ standard deviation of the corresponding signal segment. Based on the measured data, the SNR was approximately 44. Using a 1σ criterion, corresponding to SNR = 1, the LOD was calculated as:

$$LOD = \frac{C_{0.75ppm}}{SNR} \tag{7}$$

Therefore,

$$LOD = \frac{0.75ppm}{44} \approx 0.017ppm = 17ppb \tag{8}$$

Thus, the reported 17 ppb is a 1σ-based SNR-estimated LOD calculated from the experimentally measured 0.75 ppm C_2H_2 signal under a 50 s integration time, rather than a directly measured 17 ppb concentration. The main factors limiting the detection performance include the residual background noise of the QTF, electronic noise from the preamplifier and lock-in amplifier, laser intensity fluctuation, residual optical background caused by beam alignment, and gas-flow-induced acoustic disturbance. For dissolved acetylene detection, the headspace degassing efficiency and mass-transfer process may also influence the overall response and uncertainty.

To evaluate the measurement reproducibility and long-term stability of the system, a continuous measurement of 1 ppm C_2H_2 was performed under the optimized operating conditions. The QEPAS signal was continuously recorded at a sampling interval of 1 s, and a total of 3007 consecutive data points were obtained over approximately 3006 s. For the stable signal segment, the standard deviation of the measured QEPAS signal was calculated to be approximately 1.43×10^{-6} V.

The sensitivity, defined as the slope of the linear fitting curve between the QEPAS 2f signal amplitude and the C_2H_2 concentration, was calculated to be approximately 4.63×10^{-6} V/ppm in the 100–500 ppm range. For the low-concentration range of 0–1 ppm, the sensitivity was approximately 1.27×10^{-5} V/ppm. These results confirm the good linear response capability of the proposed clamp-type QEPAS system over different concentration ranges. As shown in Figure 7, the low-concentration calibration curve in the 0–1 ppm range also exhibited a good linear response, with a correlation coefficient of 0.995, further supporting the reliability of the SNR-estimated LOD calculation based on the 0.75 ppm C_2H_2 measurement.

Allan deviation analysis was further performed to determine the optimal averaging time and evaluate the stability of the sensor system. As shown in Figure 8, the Allan deviation decreased with increasing averaging time in the short-time region, indicating that random noise could be effectively suppressed by signal averaging. A minimum Allan deviation of 6.13×10^{-7} V was obtained at an averaging time of 29 s. When the averaging time was further increased, the Allan deviation gradually increased, suggesting that long-term drift began to dominate the measurement. The drift may originate from laser intensity fluctuation, a slow variation in the QTF resonance frequency, environmental temperature variation, and gas-flow-induced disturbance. These results demonstrate that the proposed

clamp-type QEPAS system exhibits good short-term reproducibility and stability, with an optimal averaging time of approximately 29 s under the present experimental conditions.

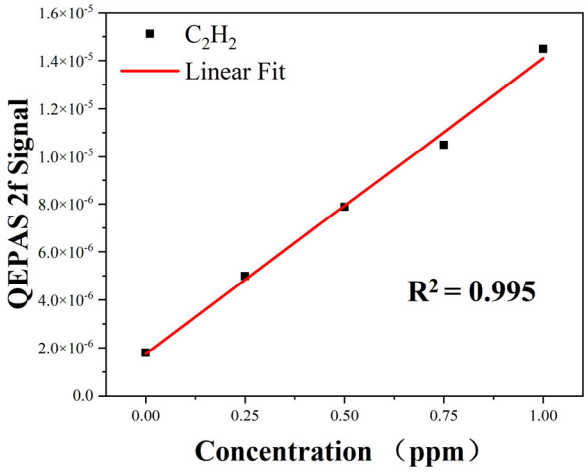


Figure 7. Linear fitting curve of the 2f signal amplitude versus low acetylene concentration.

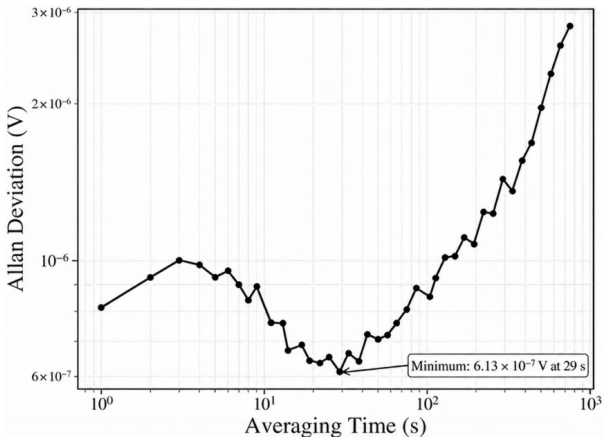


Figure 8. Allan deviation analysis of the QEPAS signal for 1 ppm C_2H_2 under the optimized operating conditions.

A comparison with representative acetylene detection methods is summarized in Table 1. Representative acetylene detection methods, including GC, TDLAS, conventional PAS, fiber-optic PAS, and QEPAS-based methods, are summarized in Table 1 to demonstrate the relative performance and application potential of the proposed clamp-type QEPAS system.

Table 1. Comparison of representative acetylene detection and related infrared spectroscopic gas sensing methods.

Detection Method	Sample Type	Response/ Averaging Time	Excitation Wavelength/ Sensing Configuration	Detection Limit	LOD Type	Ref.
Gas chromatography (GC)	Dissolved gas in transformer oil	Several minutes	Conventional DGA	ppm-level	Directly measured	[51]
Tunable diode laser absorption spectroscopy (TDLAS)	Dissolved C_2H_2 in transformer oil	Not specified	Near-infrared absorption; 1530.37 nm	0.49 ppm	Estimated/ system LOD	[3]

Table 1. *Cont.*

Detection Method	Sample Type	Response/ Averaging Time	Excitation Wavelength/ Sensing Configuration	Detection Limit	LOD Type	Ref.
Conventional resonant photoacoustic spectroscopy (PAS) with EDFA	Gas-phase C_2H_2	60 s averaging time	1532.83 nm; resonant PA cell; EDFA-enhanced excitation	0.37 ppb	1σ estimated	[52]
T-type photoacoustic cell with headspace degassing	Dissolved C_2H_2 in transformer oil	Not specified	T-type PA cell + headspace degassing	0.2 μL/L	Not specified	[53]
Fiber-optic photoacoustic sensing with headspace degassing	Dissolved C_2H_2 in transformer oil	9 min	DFB laser + EDFA + fiber-optic acoustic sensor	0.05 μL/L	Directly measured/ experimentally verified	[5]
On-beam QEPAS based on a 28 kHz QTF	Gas-phase C_2H_2	1 s	On-beam QEPAS; 28 kHz QTF + AmR	28.8 ppb	Allan/SNR estimated	[54]
High-power near-infrared QEPAS with 10 W EDFA	Gas-phase C_2H_2	Not specified	1536 nm DFB laser + 10 W EDFA + 28 kHz QTF	ppb-level	NNEA/SNR estimated	[48]
Tunable Fabry–Perot filter based on a silicon wafer	Infrared gas sensing application	Not specified	Tunable Fabry–Perot filter	Not specified	Not specified	[55]
Molecular spectroscopy analysis for NDIR sensor design	SF_6/industrial gas sensing	Not specified	NDIR spectral band analysis	Not specified	Not specified	[56]
Proposed clamp-type QEPAS system	Dissolved C_2H_2 in transformer oil	50 s integration time; ~550 s degassing plateau	1532 nm DFB laser + clamp-type QTF + acoustic micro-resonator + headspace degassing	17 ppb	SNR-estimated, SNR = 1	This work

"Not specified" indicates that the corresponding parameter was not explicitly reported in the cited work. The 17 ppb LOD reported in this work is a 1σ-based SNR-estimated value calculated from the continuous 0.75 ppm C_2H_2 measurement under a 50 s integration time, rather than a directly measured concentration.

3.4. Online Measurement of Dissolved Acetylene in Transformer Oil

To evaluate practical application, a headspace degassing system was used for online transformer oil measurements, as shown in Figure 9. The procedure involved oil pre-cleaning, evacuation to −735 Torr, injection of 500 mL transformer oil, re-evacuation, vacuum circulation, and laser measurement.

The results indicated that acetylene was detected at ~20 s, increased with time, and reached a stable peak at ~550 s. The final measured concentration was 16.2 ppm, consistent with gas chromatography measurements, confirming the effectiveness of the proposed system for dissolved gas analysis in transformer oil, as shown in Figure 10.

The dynamic response of the headspace degassing process is governed by gas diffusion in oil, interfacial desorption, gas-phase mixing, and transport to the QEPAS detection cell. The signal appeared after approximately 20 s, indicating the onset of acetylene release and transport. The subsequent increase reflects continuous mass transfer from oil to the gas phase under negative pressure. The plateau at approximately 550 s indicates that the headspace concentration approached a quasi-equilibrium state under the present oil volume, pressure, and circulation conditions.

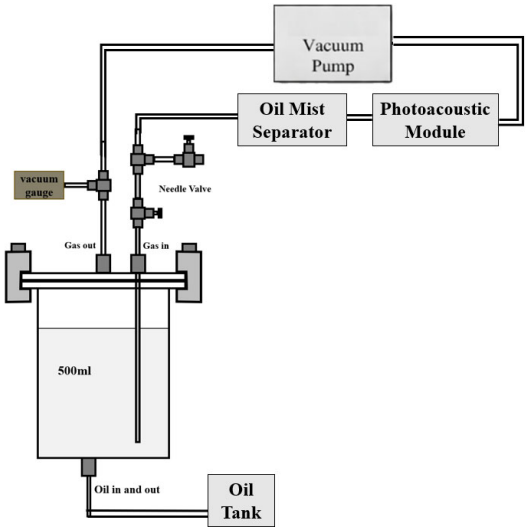


Figure 9. Schematic of the online gas measurement system integrated with the headspace degassing experimental platform.

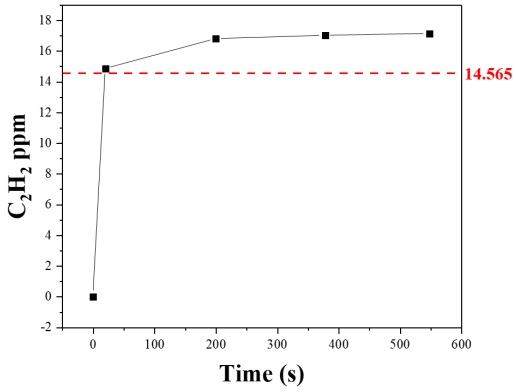


Figure 10. Real-time response curve of dissolved acetylene concentration extracted from transformer oil.

4. Discussion

In this study, a high-sensitivity quartz-enhanced photoacoustic spectroscopy (QEPAS) system based on a clamp-type quartz tuning fork was developed and integrated with a headspace degassing device for online detection of dissolved acetylene in transformer oil. The enhanced signal intensity observed under reduced pressure can be attributed to the decreased viscous damping effect of gas molecules on the QTF prongs, which leads to a narrower resonance bandwidth and a higher Q-factor. Experimental results demonstrate that the system can complete the measurement process within several minutes, achieving a detection sensitivity at the ppb level. The measured concentrations were consistent with gas chromatography (GC) results, confirming the reliability and accuracy of the proposed setup. The system's performance benefits from several factors: the clamp-type QTF provides high Q-factor and efficient acoustic coupling, significantly enhancing the photoacoustic signal; the headspace degassing effectively separates dissolved gases from oil, ensuring complete gas delivery and accurate measurements; finally, lock-in amplification and modulation depth optimization improve the signal-to-noise ratio.

Compared with the membrane-degassing-based PAS method previously reported in ref. [40], the proposed headspace-degassing clamp-type QEPAS system exhibits a lower detection limit and improved integration flexibility for online monitoring.

Despite these advantages, several aspects should be further improved. First, the current headspace degassing process limits the response time, and optimized fluidic design,

stirring, or heating may accelerate gas extraction. Second, higher-power or mid-infrared light sources could enhance molecular absorption and further improve sensitivity. Third, direct in-oil measurement may simplify the system configuration and improve real-time monitoring capability.

Although the current laboratory prototype consists of separated gas delivery, degassing, optical excitation, and signal detection modules, the core QEPAS sensing head is millimeter-scale and is therefore suitable for miniaturization [57]. Future integration can be achieved by using compact fiber-coupled lasers, miniature vacuum pumps, microvalves, integrated pressure sensors, and portable lock-in detection electronics. The main engineering challenges are the integration of the headspace degassing chamber, pressure stabilization, oil mist suppression, and vibration isolation for field operation [58].

To further clarify the advantages of the proposed clamp-type QEPAS system, representative acetylene detection methods reported in previous studies are summarized in Table 1. These methods include conventional gas chromatography, TDLAS, conventional PAS, fiber-optic PAS, and QEPAS-based techniques. Compared with conventional GC and TDLAS methods, photoacoustic-based methods generally provide higher sensitivity and stronger potential for compact online monitoring. Among them, QEPAS offers the advantages of small gas consumption, high acoustic-noise immunity, and miniaturization capability due to the use of a quartz tuning fork as a sharply resonant acoustic transducer.

Overall, this study demonstrates high sensitivity and low detection limit for dissolved gas analysis, providing a reliable foundation and clear directions for future improvements in QEPAS-based oil monitoring.

5. Conclusions

A quartz-enhanced photoacoustic spectroscopy system based on a clamp-type QTF was developed and integrated with a headspace degassing device, forming an effective platform for dissolved gas analysis in transformer oil. The system can complete acetylene measurements within minutes and achieves a 1σ-based SNR-estimated LOD of 17 ppb under a 50 s integration time. Future improvements include accelerating the degassing process to reduce response time, employing higher-power or alternative-wavelength light sources to enhance the photoacoustic signal, and exploring direct in-oil measurement to simplify the setup and enable more efficient real-time monitoring of dissolved gases.

Author Contributions: Conceptualization, Y.Z.; methodology, Y.Z.; software, G.Z.; validation, H.Z. and G.Z.; data curation, Y.Q.; Writing—original draft, Y.Q.; Writing—review & editing, Y.Q. and Q.W.; Project administration, K.J. All authors have read and agreed to the published version of the manuscript.

Funding: This research was funded by the China Southern Power Grid Co., Ltd. Science and Technology Project Fund, grant number "GDKJXM20230996(036100KC23090001)".

Data Availability Statement: Data are contained within the article.

Conflicts of Interest: Authors Yihua Qian, Yaohong Zhao and Qing Wang were employed by the company Electric Power Research Institute of Guangdong Power Grid Co., Ltd. The remaining authors declare that the research was conducted in the absence of any commercial or financial relationships that could be construed as a potential conflict of interest.

References

1. Yin, Z.; Huo, C.; Sun, H.; Chen, J. Development of Degassing Device for Transformer oil Based on Headspace Degassing Method. *Proc. E3S Web Conf.* **2021**, *252*, 02010. [CrossRef]
2. Bustamante, S.; Manana, M.; Arroyo, A.; Castro, P.; Laso, A.; Martinez, R. Dissolved gas analysis equipment for online monitoring of transformer oil: A review. *Sensors* **2019**, *19*, 4057. [CrossRef] [PubMed]

3. Ma, G.-m.; Zhao, S.-j.; Jiang, J.; Song, H.-t.; Li, C.-r.; Luo, Y.-t.; Wu, H. Tracing acetylene dissolved in transformer oil by tunable diode laser absorption spectrum. *Sci. Rep.* **2017**, *7*, 14961. [CrossRef] [PubMed]
4. Ali, M.S.; Omar, A.; Jaafar, A.S.A.; Mohamed, S.H. Conventional methods of dissolved gas analysis using oil-immersed power transformer for fault diagnosis: A review. *Electr. Power Syst. Res.* **2023**, *216*, 109064. [CrossRef]
5. Chen, K.; An, R.; Li, C.; Kang, Y.; Ma, F.; Zhao, X.; Guo, M.; Qi, H.; Zhao, J. Detection of ultra-low concentration acetylene gas dissolved in oil based on fiber-optic photoacoustic sensing. *Opt. Laser Technol.* **2022**, *154*, 108299. [CrossRef]
6. Zhang, Q.; Li, B.; Du, X.; Wei, Y.; Zhang, T.; Gong, W.; Wang, Z.; Liu, G. Intra-cavity QEPAS gas sensor based on fiber-ring laser for C2H2 detection. In *Proceedings of the AOPC 2022: Infrared Devices and Infrared Technology; and Terahertz Technology and Applications*; SPIE: Bellingham, WA, USA, 2023; pp. 92–96.
7. Sun, H.-C.; Huang, Y.-C.; Huang, C.-M. A review of dissolved gas analysis in power transformers. *Energy Procedia* **2012**, *14*, 1220–1225. [CrossRef]
8. Kaysir, M.R.; Zaman, T.M.; Rassel, S.; Wang, J.; Ban, D. Photoacoustic resonators for non-invasive blood glucose detection through photoacoustic spectroscopy: A systematic review. *Sensors* **2024**, *24*, 6963. [CrossRef]
9. Li, B.; Menduni, G.; Giglio, M.; Patimisco, P.; Sampaolo, A.; Zifarelli, A.; Wu, H.; Wei, T.; Spagnolo, V.; Dong, L. Quartz-enhanced photoacoustic spectroscopy (QEPAS) and Beat Frequency-QEPAS techniques for air pollutants detection: A comparison in terms of sensitivity and acquisition time. *Photoacoustics* **2023**, *31*, 100479. [CrossRef]
10. Chang, E.-Q.; Wang, G.; Li, Y.-F.; Yu, Y.; Wang, Y.; Lu, Z. Study on research progress of quartz-enhanced photoacoustic spectroscopy for trace gas detection. *Front. Phys.* **2025**, *13*, 1709349. [CrossRef]
11. Wijesinghe, D.R.; Zobair, M.A.; Esmaeelpour, M. A review on photoacoustic spectroscopy techniques for gas sensing. *Sensors* **2024**, *24*, 6577. [CrossRef]
12. Wang, L.; Lv, H.; Zhao, Y.; Wang, C.; Luo, H.; Lin, H.; Xie, J.; Zhu, W.; Zhong, Y.; Liu, B. Sub-ppb level HCN photoacoustic sensor employing dual-tube resonator enhanced clamp-type tuning fork and U-net neural network noise filter. *Photoacoustics* **2024**, *38*, 100629. [CrossRef]
13. Qiao, S.; He, Y.; Sun, H.; Patimisco, P.; Sampaolo, A.; Spagnolo, V.; Ma, Y. Ultra-highly sensitive dual gases detection based on photoacoustic spectroscopy by exploiting a long-wave, high-power, wide-tunable, single-longitudinal-mode solid-state laser. *Light Sci. Appl.* **2024**, *13*, 100. [CrossRef] [PubMed]
14. Lin, H.; Zheng, H.; Zhu, W.; Zhong, Y.; Yu, J.; Wu, H.; Jia, Z.; Zhang, J.; Sampaolo, A.; Patimisco, P. Multifunctional lithium niobate platform for photodetection and photoacoustic and thermoelastic gas sensing. *Nat. Commun.* **2026**, *17*, 2296. [CrossRef]
15. Zhuang, R.; He, J.; Lin, H.; Luo, H.; Lin, L.; Wang, L.; Liu, B.; Zhu, W.; Zhong, Y.; Yu, J. Conductance-photoacoustic spectroscopy for fast and concurrent sensing of hydrogen and hydrocarbons. *Photoacoustics* **2025**, *45*, 100752. [CrossRef]
16. Zhang, S.; Cao, Y.; Li, C.; Wang, R.; Wang, G.; Liu, K.; Gao, X. Sub-ppb level photoacoustic spectroscopy NOx sensor using a low cost 455 nm laser diode. *Sens. Actuators B Chem.* **2025**, *441*, 138039. [CrossRef]
17. Zhang, R.; Dias, M.; Li, Y.; Rütten, S.; Kiessling, F.; Lammers, T.; Pallares, R.M. Structural engineering of silver nanoparticles for enhanced photoacoustic imaging. *Nanoscale Adv.* **2025**, *7*, 6110–6119. [CrossRef] [PubMed]
18. Zhang, C.; Qiao, S.; He, Y.; Liu, C.; Ma, Y. Multi-resonator T-type photoacoustic cell based photoacoustic spectroscopy gas sensor for simultaneous measurement C_2H_2, CH_4 and CO_2. *Sens. Actuators B Chem.* **2025**, *427*, 137168. [CrossRef]
19. Zha, S.; Chen, H.; Liu, C.; Guo, Y.; Ma, H.; Zhang, Q.; Li, L.; Zhan, S.; Cheng, G.; Cao, Y. Multivariate-coupled-enhanced photoacoustic spectroscopy with Chebyshev rational fractional-order filtering algorithm for trace CH4 detection. *Photoacoustics* **2025**, *42*, 100692. [CrossRef]
20. Yin, X.; Zhu, C.; Yang, X.; Xu, K.; Liang, Y.; Zhang, D.; Mao, W.; Wu, H. Trace photoacoustic spectroscopy gas sensors for COx detection. *Measurement* **2025**, *262*, 120059. [CrossRef]
21. Wu, G.; Guan, Y.; Jiang, J.; Xing, J.; Gong, Z. A Dual-Enhancement Fiber-Optic Photoacoustic Spectroscopy Sensor Based on a Spherical–Cylindrical Coupled Resonator with an Integrated Multipass Cell for Sub-ppb C_2H_2 Detection. *Anal. Chem.* **2025**, *97*, 20543–20548. [CrossRef]
22. Wang, W.; Zhang, T.; Zhang, Q.; Feng, Y.; Wei, Y.; Wang, L.; Gu, Y.; Li, C. Photoacoustic spectroscopy two-component gas sensing system based on a semi-ellipsoidal resonant photoacoustic cell. *Sens. Actuators B Chem.* **2025**, *446*, 138616. [CrossRef]
23. Puranika, K.S.; Malshetty, M.B.; Mooliyil, M.G.; Dehury, B.; Mazumder, N. Toward noninvasive precision: A meta-analysis of photoacoustic spectroscopy in breast cancer. *Lasers Med. Sci.* **2025**, *40*, 461. [CrossRef]
24. Petrus, M.; Popa, C.; Bratu, A.M.; Bercu, V.; Gebac, L.; Mihai, D.-M.; Butcaru, A.-C.; Stanica, F.; Gogot, R. A Synergistic Approach Using Photoacoustic Spectroscopy and AI-Based Image Analysis for Post-Harvest Quality Assessment of Conference Pears. *Molecules* **2025**, *30*, 2431. [CrossRef] [PubMed]
25. Meng, Z.; Xiang, J.; Li, W.; Xia, L.; Guo, W.; Xia, M.; Yang, K. Multicomponent gas measurement method based on miniaturized and scalable multiresonator photoacoustic spectroscopy. *Anal. Chem.* **2025**, *97*, 4158–4165. [CrossRef]

26. Melchiorre, L.; Anelli, F.; Menduni, G.; Annunziato, A.; Bodin, L.; Cozic, S.; Magno, G.; Sampaolo, A.; Prudenzano, F.; Spagnolo, V. Dual-gas quartz-enhanced photoacoustic spectroscopy sensor exploiting two fiber-combined interband cascade lasers. *Photoacoustics* **2025**, *42*, 100689. [CrossRef]
27. Lin, C.; Zhang, X.; Yan, X.; Cai, Y.; Li, W. Part-per-billion (ppb)-level acetylene sensor employing optical quartz enhanced photoacoustic spectroscopy (QEPAS) with an erbium-doped fiber amplifier (EDFA) and a fiber-optic Fabry–Perot interferometer. *Anal. Lett.* **2025**, *58*, 2233–2248. [CrossRef]
28. Jothimani, D.; Manoharan, M.; Rela, M.; Selvaraj, R.; Seshadri, S.; Sm, S.N.; Vasa, N.J. Quartz-enhanced photoacoustic spectroscopy-based acetone and ammonia measurements from human breath near 8 μm wavelength band. *ACS Sens.* **2025**, *10*, 254–263.
29. Hussain, S.A.; Singha, A.K.; Jana, B.; Mandal, P.; Sanki, P.K. An advanced IoT-based non-invasive in vivo blood glucose estimation exploiting photoacoustic spectroscopy with SDNN architecture. *Sens. Actuators A Phys.* **2025**, *387*, 116391.
30. He, Y.; Qiao, S.; Lang, T.; Zhang, C.; Qi, H.; Huang, W.; Ma, Y. Optical component-free dual-gas quartz-enhanced photoacoustic spectroscopy sensor based on highly integrated interband cascade lasers. *ACS Sens.* **2025**, *10*, 5238–5244. [CrossRef]
31. Escher, L.; Rück, T.; Jobst, S.; Pangerl, J.; Bierl, R.; Matysik, F.-M. Photodissociation-driven photoacoustic spectroscopy with UV-LEDs for ozone detection. *Photoacoustics* **2025**, *43*, 100718. [CrossRef]
32. Liu, H.; Chen, X.; Hu, M.; Wang, H.; Yao, L.; Xu, Z.; Ma, G.; Wang, Q.; Kan, R. In situ high-precision measurement of deep-sea dissolved methane by quartz-enhanced photoacoustic and light-induced thermoelastic spectroscopy. *Anal. Chem.* **2024**, *96*, 12846–12853. [CrossRef]
33. Chen, X.; Chen, X.; Yao, L.; Hu, M.; Liu, H.; Kan, R. Chirp-modulated light-induced thermoelastic spectroscopy for simultaneous precise measurement of resonant frequency and gas concentration. *Photoacoustics* **2026**, *48*, 100812. [CrossRef]
34. Das, S.; Fernandes, R.; Karhu, J.; Hrovat, B.; Koistinen, A.; Martins, R.; Marques, C.; Toivonen, J.; Ikonen, E. Identification of microplastics with cantilever enhanced photoacoustic spectroscopy in infrared region. *J. Environ. Chem. Eng.* **2025**, *13*, 118556. [CrossRef]
35. Chen, Y.; Ma, H.; Qiao, S.; He, Y.; Fang, C.; Li, Q.; Zhou, S.; Ma, Y. Rapid ppb-Level methane detection based on quartz-enhanced photoacoustic spectroscopy. *Anal. Chem.* **2025**, *97*, 6780–6787. [CrossRef] [PubMed]
36. Patimisco, P.; Scamarcio, G.; Tittel, F.K.; Spagnolo, V. Quartz-enhanced photoacoustic spectroscopy: A review. *Sensors* **2014**, *14*, 6165–6206. [CrossRef] [PubMed]
37. Wang, Z.; Wang, Q.; Zhang, H.; Borri, S.; Galli, I.; Sampaolo, A.; Patimisco, P.; Spagnolo, V.L.; De Natale, P.; Ren, W. Doubly resonant sub-ppt photoacoustic gas detection with eight decades dynamic range. *Photoacoustics* **2022**, *27*, 100387. [CrossRef] [PubMed]
38. Votintsev, A.P.; Borisov, A.V.; Makashev, D.R.; Stoyanova, M.Y.; Kistenev, Y.V. Quartz-enhanced photoacoustic spectroscopy in the terahertz spectral range. *Photonics* **2023**, *10*, 835. [CrossRef]
39. Li, C.; Chen, K.; Zhao, J.; Qi, H.; Zhao, X.; Ma, F.; Han, X.; Guo, M.; An, R. High-sensitivity dynamic analysis of dissolved gas in oil based on differential photoacoustic cell. *Opt. Lasers Eng.* **2023**, *161*, 107394. [CrossRef]
40. Rasmussen, A.N.; Thomsen, B.L.; Christensen, J.B.; Petersen, J.C.; Lassen, M. Quartz-enhanced photoacoustic spectroscopy assisted by partial least-squares regression for multi-gas measurements. *Sensors* **2023**, *23*, 7984. [CrossRef]
41. Sampaolo, A.; Patimisco, P.; Giglio, M.; Zifarelli, A.; Wu, H.; Dong, L.; Spagnolo, V. Quartz-enhanced photoacoustic spectroscopy for multi-gas detection: A review. *Anal. Chim. Acta* **2022**, *1202*, 338894. [CrossRef]
42. Shi, Y.; Gu, P.; Zhao, M.; Han, Y. Rapid online detection of dissolved acetylene in transformer oil by photoacoustic spectroscopy and membrane degassing. *Electr. Eng.* **2025**, *107*, 3075–3081. [CrossRef]
43. Wei, T.; Zifarelli, A.; Dello Russo, S.; Wu, H.; Menduni, G.; Patimisco, P.; Sampaolo, A.; Spagnolo, V.; Dong, L. High and flat spectral responsivity of quartz tuning fork used as infrared photodetector in tunable diode laser spectroscopy. *Appl. Phys. Rev.* **2021**, *8*, 041409. [CrossRef]
44. Qiao, S.; Ma, Y.; He, Y.; Patimisco, P.; Sampaolo, A.; Spagnolo, V. Ppt level carbon monoxide detection based on light-induced thermoelastic spectroscopy exploring custom quartz tuning forks and a mid-infrared QCL. *Opt. Express* **2021**, *29*, 25100–25108. [CrossRef]
45. Sun, B.; Zifarelli, A.; Wu, H.; Dello Russo, S.; Li, S.; Patimisco, P.; Dong, L.; Spagnolo, V. Mid-infrared quartz-enhanced photoacoustic sensor for ppb-level CO detection in a SF6 gas matrix exploiting a T-grooved quartz tuning fork. *Anal. Chem.* **2020**, *92*, 13922–13929. [CrossRef] [PubMed]
46. Wu, Q.; Lv, H.; Lin, L.; Wu, H.; Giglio, M.; Zhu, W.; Zhong, Y.; Sampaolo, A.; Patimisco, P.; Dong, L. Clamp-type quartz tuning fork enhanced photoacoustic spectroscopy. *Opt. Lett.* **2022**, *47*, 4556–4559. [CrossRef] [PubMed]
47. Ma, Y.; He, Y.; Patimisco, P.; Sampaolo, A.; Qiao, S.; Yu, X.; Tittel, F.K.; Spagnolo, V. Ultra-high sensitive trace gas detection based on light-induced thermoelastic spectroscopy and a custom quartz tuning fork. *Appl. Phys. Lett.* **2020**, *116*, 011103. [CrossRef]

48. Yang, Z.; Lin, H.; Montano, B.A.Z.; Zhu, W.; Zhong, Y.; Yuan, B.; Yu, J.; Kan, R.; Shao, M.; Zheng, H. High-power near-infrared QEPAS sensor for ppb-level acetylene detection using a 28 kHz quartz tuning fork and 10 W EDFA. *Opt. Express* **2022**, *30*, 6320–6331. [CrossRef] [PubMed]
49. Dai, J.; Luo, B.; Shen, X.; Han, W.; Cui, R.; Wu, J.; Zhang, H.; Xiao, W.; Zhong, Z.; Dong, L. A review of optical gas sensing technology for dissolved gas analysis in transformer oil. *Front. Phys.* **2025**, *13*, 1547563. [CrossRef]
50. Li, Z.; Zhang, Q.; Wang, Z.; Dai, J. A highly sensitive low-pressure TDLAS sensor for detecting dissolved CO and CO_2 in transformer insulating oil. *Opt. Laser Technol.* **2024**, *174*, 110622. [CrossRef]
51. *ASTM D3612*; Standard Test Method for Analysis of Gases Dissolved in Electrical Insulating Oil by Gas Chromatography. ASTM International: West Conshohocken, PA, USA, 2017.
52. Chen, K.; Gong, Z.; Yu, Q. Fiber-amplifier-enhanced resonant photoacoustic sensor for sub-ppb level acetylene detection. *Sens. Actuators A Phys.* **2018**, *274*, 184–188. [CrossRef]
53. Wang, G.; Fu, D.; Yuan, S.; Li, C.; Han, X.; Du, J.; Du, F.; Chen, K. Rapid detection of dissolved acetylene in oil based on T-type photoacoustic cell. *Microw. Opt. Technol. Lett.* **2024**, *66*, e33793. [CrossRef]
54. Lin, H.; Zheng, H.; Montano, B.A.Z.; Wu, H.; Giglio, M.; Sampaolo, A.; Patimisco, P.; Zhu, W.; Zhong, Y.; Dong, L. Ppb-level gas detection using on-beam quartz-enhanced photoacoustic spectroscopy based on a 28 kHz tuning fork. *Photoacoustics* **2022**, *25*, 100321. [CrossRef] [PubMed]
55. Ramos-Gonzalez, D.A.; Gallegos-Arellano, E.; Salcedo-Rodriguez, C.A.; Avila-Garcia, M.S.; Reyes-Ayona, J.R.; Avina-Ortiz, J.R.; Avina-Bravo, E.G.; Sierra-Hernandez, J.M. Design of a tunable Fabry–Perot filter based on a silicon wafer for gas sensing applications in the infrared. *Infrared Phys. Technol.* **2025**, *145*, 105689. [CrossRef]
56. Salcedo-Rodríguez, C.A.; Gallegos-Arellano, E.; Hernández-Garcia, J.C.; Ramos-Gonzalez, D.A.; Estrada-Pintor, M.I.; Avila-Garcia, M.S.; Delgado-Arredondo, P.A.; Sierra-Hernandez, J.M. Molecular spectroscopy analysis of SF6 absorption bands for the design of highly sensitive NDIR sensors for industrial applications. *Measurement* **2025**, *258*, 119169. [CrossRef]
57. Pan, Y.; Fu, L.; Zhang, J.; Lu, P. Open-closed single-tube on-beam tuning-fork-enhanced fiber-optic photoacoustic spectroscopy. *Photoacoustics* **2024**, *39*, 100639. [CrossRef]
58. Pan, Y.; Lu, P.; Cheng, L.; Li, Z.; Liu, D.; Zhao, J.; Wang, Y.; Fu, L.; Sima, C.; Liu, D. Miniaturized and highly-sensitive fiber-optic photoacoustic gas sensor based on an integrated tuning fork by mechanical processing with dual-prong differential measurement. *Photoacoustics* **2023**, *34*, 100573. [CrossRef] [PubMed]

Disclaimer/Publisher's Note: The statements, opinions and data contained in all publications are solely those of the individual author(s) and contributor(s) and not of MDPI and/or the editor(s). MDPI and/or the editor(s) disclaim responsibility for any injury to people or property resulting from any ideas, methods, instructions or products referred to in the content.